



# Mechanical hardness estimation of heat-treated DIN50Cr3 spring steel utilizing laser-induced breakdown spectroscopy (LIBS) inverse calibration

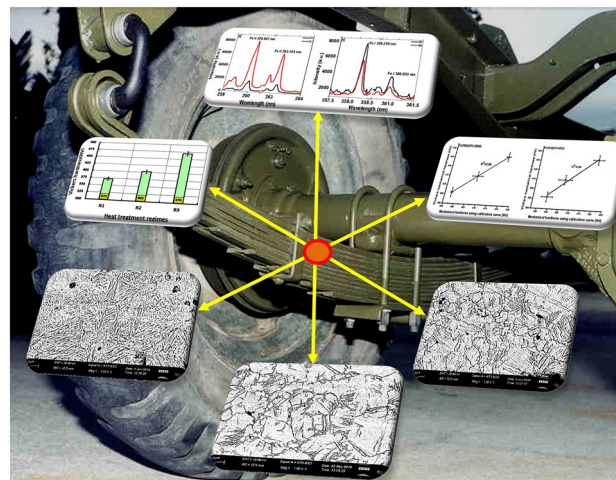
Mohamed M. ElFaham<sup>1</sup> · Waled M. Elthalabawy<sup>2</sup> · O. Elzahed<sup>2</sup> · Mohamed A. Zakaria<sup>3</sup> · M. Abdelhamid<sup>4</sup>

Received: 23 October 2019 / Accepted: 28 January 2020  
© Springer-Verlag GmbH Germany, part of Springer Nature 2020

## Abstract

In various industrial applications, particularly for suspension systems, a range of mechanical properties are required to meet the designer requirements. In the present work, the semi-nondestructive laser-induced breakdown spectroscopy (LIBS) technique was used for the first time to estimate the hardness (HV units) of the light duty low-carbon spring steel DIN50Cr3 through LIBS calibration curves. For this purpose, three distinct spring steel samples, namely DIN50Cr3 were successfully treated by subjecting to various treatment regimes, namely R1 annealing, R2 quenching and R3 normalizing. The calibration curves were constructed using the ratio of ionic to atomic line intensities of LIBS spectra versus the Vickers mechanical hardness as well as microstructural analyses were performed. The mechanical hardness for spring steel DIN50Cr3 subjected to different tempering heat treatment regimes R4, R5 and R6 is then deduced from the calibration curves, and their values were correlated with those obtained from Vickers test. Microstructural analysis was performed using scanning electron microscopy (SEM) and correlated the variation of the obtained hardness level to the microstructural changes accompanying all heat treatment regimes.

## Graphic abstract



**Keywords** LIBS calibration curve · Spring steel DIN 50Cr3 · Surface hardness · Heat treatment regimes · SEM · Vickers test

Mohamed M. ElFaham and Waled M. Elthalabawy contributed equally to this article.

Extended author information available on the last page of the article

## 1 Introduction

Laser-induced breakdown spectroscopy (LIBS) has accomplished a stunning growth in the last decade. Recently researchers investigated the use of LIBS in several laboratories around the world, almost around 50 years have passed during a remarkable progress has been achieved. LIBS is a well-known analytical technique used for fast and easy elemental analysis of solids, liquids and gases [1–3]. Briefly, in LIBS analysis, a high-intense laser pulse is focused onto the surface of the target; a tiny amount of the material is ablated, vaporized and through further photon absorption is heated up until it ionizes forming plasma. This laser-induced plasma is considered as a micro-source of light that can be analyzed to identify the elements evaporated from the material under investigation. Whereas many other analytical techniques require significant sample preparation like inductively coupled plasma, mass spectrometry (ICP-MS) and atomic absorption spectroscopy (AAS), LIBS requires no sample preparation. LIBS technique was successfully tested in a wide range of applications including industry sector [4–6], military sector [7] environmental monitoring [8, 9], cultural heritage analysis [10, 11], and underwater analysis [12].

In the recent years, LIBS provides a powerful mean for spectroscopic determination of mechanical characteristics of metal alloys such as hardness [13–15] and surface resistance against mechanical wear [16, 17]. The ability of applying LIBS technique in hardness evaluation provides a semi-nondestructive and powerful alternative technique relative to the conventional mechanical indentation methods such as Brinell, Vickers and Rockwell hardness tests [18–21]. It was proved that the ratio of ionic to atomic spectral line intensities is well correlated with the Vickers macro-indentation hardness.

Moreover, the LIBS technique revealed a high accuracy linear relation between the ratio of ionic to atomic spectral line intensities and the concrete compressive strength [22]. A similar method, but using the first, second and the third harmonics of Nd: YAG laser, has been utilized on Fe–V–C metallic alloys of different compositions [23].

On the other hand, one of the most important steel alloys in the industrial applications is the spring steel alloy. They are generally having low-, medium- or high-carbon steels. Chromium, manganese and silicon are the major alloying elements that were added to improve the elastic properties of these steel grades. The addition of these elements provides remarkable effect on hardness, strength, ductility and toughness [24, 25].

While small spring sizes can be directly formed in the hardened state, larger spring sizes are formed in the annealed state, where the material has sufficient level

of ductility, and then thermal treatments are carried out after forming to improve its mechanical characteristics. The objective of thermal treatment of these steel grades is mainly directed to enlarge the elastic range and to increase the ratio between yield and ultimate strength ( $\sigma_y/\sigma_u$ ) [26]. In general, quenching and tempering thermal treatment cycles are means that produce strengthening effect of these steels. This is mainly achieved through forming a martensitic structure by quenching and a subsequent precipitation of fine dispersion of alloy carbides during tempering [27].

The martensitic structure is rarely used in a non-tempered condition because the high internal stresses associated with this transformation causes some deficiency to the alloy ductility. The microstructural changes and strength variations after these thermal treatment processes depend on the cooling rate obtained during quenching. It is evident that the severity of cooling associated with using water and salt paths limited the application of these cooling media when treating spring steels. This limitation dates back to the possibility of generating cracks on the steel surface that deteriorate the mechanical properties and reduce the fatigue life of the spring [28]. Oil quenching is characterized by a relatively slower rate of cooling than water and salt paths, where it has a lower severity coefficient than both of them. Furthermore, cooling using a relative lower severity medium provides reasonable ductility, high toughness and sufficient strength levels. Oil also has the ability to tolerate the addition of any additives that can be useful in improvement of surface hardening, corrosion resistance and reducing surface cracking [29].

The objective of this work is to utilize LIBS technique for the first time as semi-nondestructive mean in hardness estimation (Vickers unit value) of thermally treated DIN50Cr3 spring steel. In this sense, calibration curves are constructed relating on a known hardness data obtained using Vickers indentation test for annealed, normalized and quenched group of samples. Verification of the success of this technique in hardness estimation was implemented by comparing the LIBS hardness values relative to Vickers mechanical indentation values. This technique was implemented for three specimen groups treated by different tempering regimes. In addition, microstructural analyses using SEM are also applied to correlate the mechanical hardness variations with the microstructural features after various treatment cycles.

## 2 Experimental work

### 2.1 Materials

The material used in this study was DIN50Cr3 spring steel. The X-Ray fluorescence (Nitkon XL3t 800) and spark

emission spectroscopy (Oxford) were used to validate the chemical composition of this alloy and revealed an alloy content of (97.96% Fe, 0.25% C, 0.2% Si, 0.79% Mn and 0.8% Cr). This material was received in the form of stripes having 6-mm thickness and 60-mm width in the annealed condition. For LIBS, microstructure and mechanical evaluations groups of 6 specimens each having  $20 \times 20 \times 6$  mm were cut and thermally treated according to the regimes shown in Table 1. The austenitization temperature for this alloy was determined to be 870 °C according to a previously published work [29]. Metallographic examination is performed using Carl Zeiss model Evo 15 scanning electron microscope. Metallography was carried out on samples from all thermally treated regimes after grinding using series of emery papers up to grit 1200 and polishing using diamond suspension down to 1 $\mu$ . Polished specimens were then etched using the standard Nital etchant [28]. Mechanical hardness evaluations were performed using Vickers hardness tester type Instron. In this technique of hardness evaluation, the polished surface is subjected to indentation by squared upright diamond pyramid using static force ( $F = 30$  kg) and dwell time of 15 s. The area of impression is calculated by determining the mean diagonal length [ $D = (d_1 + d_2)/2$ ] and substituting in Eqs. (1) and (2) [30].

$$\text{Hardness number} = \frac{\text{Applied force(kg)}}{\text{Surface area of impression(mm}^2\text{)}}, \quad (1)$$

$$\text{HV} = \frac{2F \sin\left(\frac{136}{2}\right)}{D^2} = 1.854 \frac{F}{D^2}. \quad (2)$$

## 2.2 LIBS setup

In LIBS setup, a Nd:YAG laser (Continuum laser, PL9000, USA) of a spot diameter of 0.6 mm delivers 90 mJ/pulse energy at a fundamental wavelength of 1064 nm with 5-ns pulse duration, and a repetition rate of 20 Hz has been used. This setup is similar to the one used before in a previous research work where measurements relied on a calibrated power meter (Ophir, model 1z02166) [31].

The laser pulse is focused on the sample using a plano-convex quartz lens of 5-cm focal length for plasma creation in air at atmospheric pressure. The light emitted from plasma plume was then collected through an optical fiber cable of diameter 0.6 mm at a distance of 0.5 cm from the target surface. The emitted light is then fed into a high-resolution monochromator (Acton SP2500i, 2400 lines/mm grating, a scan range from 249 to 270 nm and from 349 to 370 nm) that was used to analyze the emanated light. The gate and delay of the ICCD camera (PI MAX, 1KRB-FG-43, 1024  $\times$  1024 pixels with compatible software) were attuned to be 1.5  $\mu$ s and 2  $\mu$ s, respectively.

To assure precise measurements, calibration of the spectrometer has been achieved before evaluation. The intensifier gain of the ICCD was maintained at 900. For statistical analysis, an average of five spectra was taken for three different positions (five laser shots per position) on each sample after two laser pulses taken for cleaning. Data acquisition and spectroscopic analysis have been performed using LIBS++ and origin software.

## 3 Results and discussion

### 3.1 LIBS Calibration curves

In this section, laser-induced breakdown spectroscopy technique has been used as a verification method for the surface hardness (HV). The method was applied in terms of generation of calibration curves for DIN50Cr3 spring steel. To provide a calibration curve that can cover a range of hardness values, three distinct heat treatment regimes R1, R2 and R3 (Table 1) were utilized. LIBS spectra in two different spectral windows for spring steel sample treated according R1 and R3 regimes are shown in Fig. 1a, b. As it can be seen from Fig. 1a that the intensity of ionic emission lines was treated according to (R3) is much higher than that of treated according to (R1) (the emission line Fe II at 259.94 nm was approximated to 260 nm for better reading in the text and figures), however, on the same spectrum in another spectral window, the atomic emission lines of R1 is higher than that of R3 Fig. 1b. Furthermore, the effect of

**Table 1** Heat treatment regimes

Regime	Treatment	Treatment parameters
R1	Annealing	Austenitization at 870 °C for 1 h then furnace cooling
R2	Normalizing	Austenitization at 870 °C for 1 h then air cooling
R3	Hardening	Austenitization at 870 °C for 1 h then oil quenched to room temperature
R4	Tempering	Quenching + tempering at 250 °C for 1 h then air cooled
R5	Tempering	Quenching + tempering at 450 °C for 1 h then air cooled
R6	Tempering	Quenching + tempering at 550 °C for 1 h then air cooled

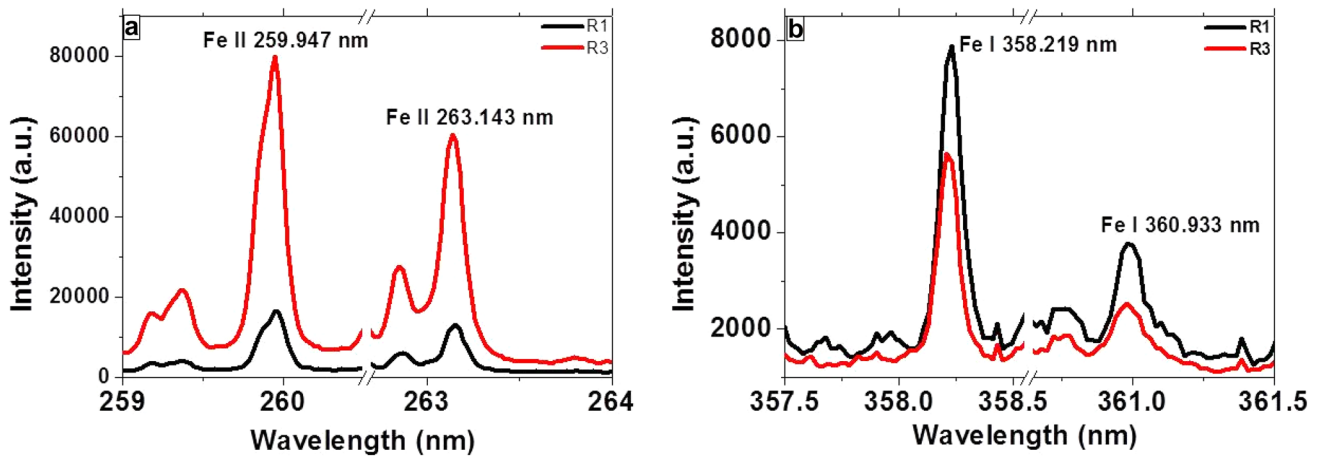


Fig. 1 LIBS signal dependence on surface hardness. **a** Ionic emission lines, **b** atomic emission lines

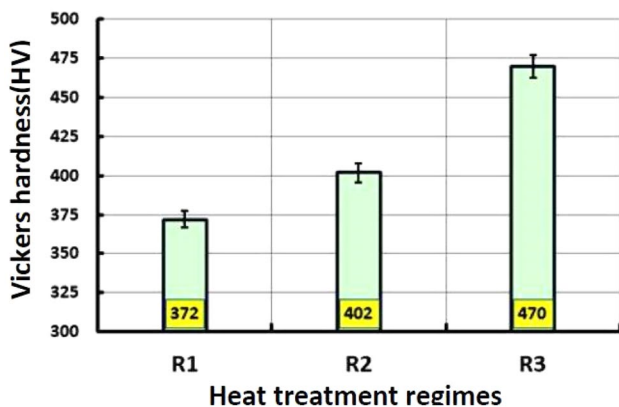


Fig. 2 Vickers hardness values of DIN50Cr3 specimens after R1, R2 and R3 regimes

the various heat-treated regimes on the mechanical hardness using Vickers indentation testing was illustrated by Fig. 2. For each heat-treated regime, the hardness value and the corresponding error bar for each condition were determined by taking the mean and the standard deviation of five readings (indentations) according to the ASM standard [32]. Calibration curves were generated using the ionic–atomic ratio in LIBS spectra versus the mechanical hardness. Ratios of Fe260(II)/Fe360(I), Fe263(II)/Fe360(I), Fe 260(II)/Fe358(I) and Fe 263(II)/Fe358(I) were used and are shown in Fig. 3. As it is clear, the results reveal that by increasing the surface hardness of the material, the ratio of ionic to atomic line intensities for a specific element is also increased. This can be attributed to the fact that the strong repulsive force between the plasma species leads to faster shock waves, strong collisions and higher plasma temperature in harder materials with lower mass removal. This in turn increases the degree of ionization and consequently, the ionic to

atomic ratio increases [33–35]. It has been also reported that plasma temperature can be considered as another factor for the proportionality between the ionic/atomic ratio and consequently with hardness measurements which provides a good linear results as well [13, 23].

Moreover, the figure depicts that there is good proportionality ( $R^2$  of 0.99 in all cases) between the intensity ratio of the ionic to atomic lines Fe II/Fe I and hardness values measured using Vickers test. In this sense, the linear relation provides a reliable calibration line that can be used for the determination of the unknown hardness of other spring steel samples subjected to different heat treatment regimes. The method is easily applicable by just knowing the Fe II/Fe I ratio of the same iron emission lines from their corresponding LIBS spectra of similar spring steel.

### 3.2 Microstructural evaluation of the spring steel reference samples

It can be noticed that the annealed specimens (R1) provide an average hardness value of 372 HV. This level of hardness is relatively low and can be attributed to the effect of annealing treatment in stress relieving, increasing ductility and decreasing the dislocation density, [22]. The microstructure of such specimens shown in Fig. 4a revealed limited amount of pearlite (P) grains and a dominant ferrite ( $\alpha$ ) matrix with an average grain size of about 25  $\mu\text{m}$ . The limited amount of pearlite is due to the low level of carbon content.

On the other hand, normalizing treatment (R2) of the same steel revealed an increase in the hardness value to reach an average of 402 HV. The increase in the hardness value can be related to the relatively high rate of air cooling that increases the dislocation density, [29]. In addition, the microstructure of the normalized specimens shown in Fig. 4b indicates a relatively smaller and uniform ferritic

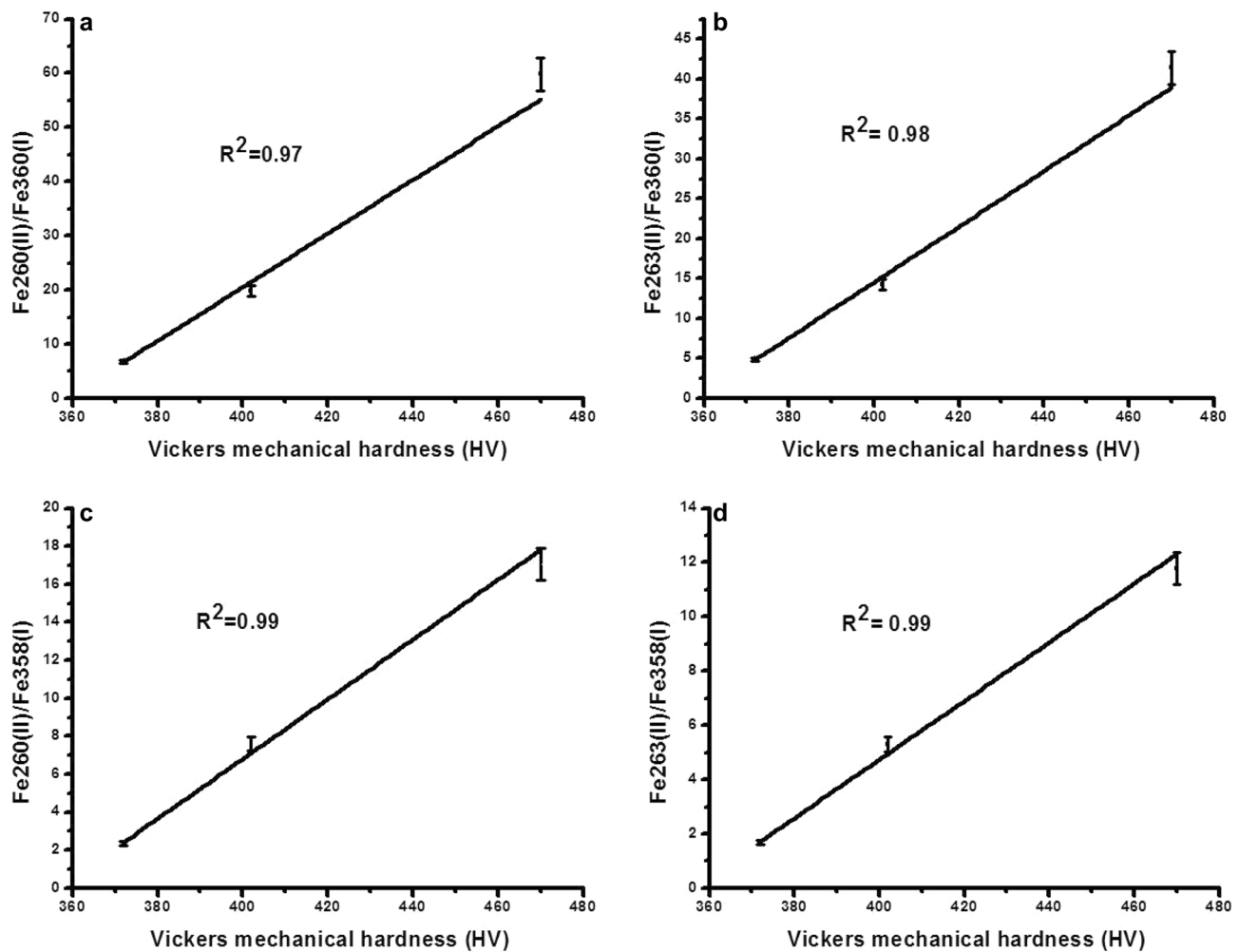


**Fig. 3** Iron ionic–atomic intensity ratio versus Vickers hardness of DIN50Cr3 treated alloys. **a** Fe 260 (II)/Fe 360(I), **b** Fe 263 (II)/Fe 360(I), **c** Fe 260(II)/Fe358(I), **d** Fe 263(II)/Fe358(I)

( $\alpha$ ) grain size, while pearlite (P) is still presented. However, the hardening condition (R3) increases the hardness of such steel to reach a maximum average value of 470 HV. The SEM micrograph Fig. 4c indicated that the high rate of cooling by oil quenching exceeded the critical rate and as a result, a structure containing lath martensite patches (M) was revealed. This morphology of martensite can be related to the low carbon content (0.25%), [29].

### 3.3 Validation of LIBS calibration curves for hardness estimation

In this section, the LIBS calibration curves obtained before in Sect. 3.1 have been used for the first time to estimate the mechanical hardness values for the DIN50Cr3-treated spring steel samples. For this purpose, a so-called “inverse calibration” is, therefore, performed. As this grade of steel

is generally used in practice in the tempered state, three different practical tempering treatments R4, R5 and R6 were performed. The values of mechanical hardness for the tempered treated samples from the calibration curves were deduced and summarized in Table 2. For more confirmation, the same samples were measured using Vickers test. It has been found that quenching and tempering treatment as defined by R4, R5 and R6 regimes in Table 1 decreases the hardness values of selected spring steel to reach 432 HV, 410 HV and 392 HV, respectively. Figure 5 represents a relation between the deduced values of mechanical hardness using LIBS calibration versus the measured values using Vickers test. The figure shows that there is good correlation with  $R^2$  of 0.99 for Fe260(II)/Fe360(I) and 0.96 for Fe263(II)/Fe360(I). This result confirms the reproducibility of the measurement.

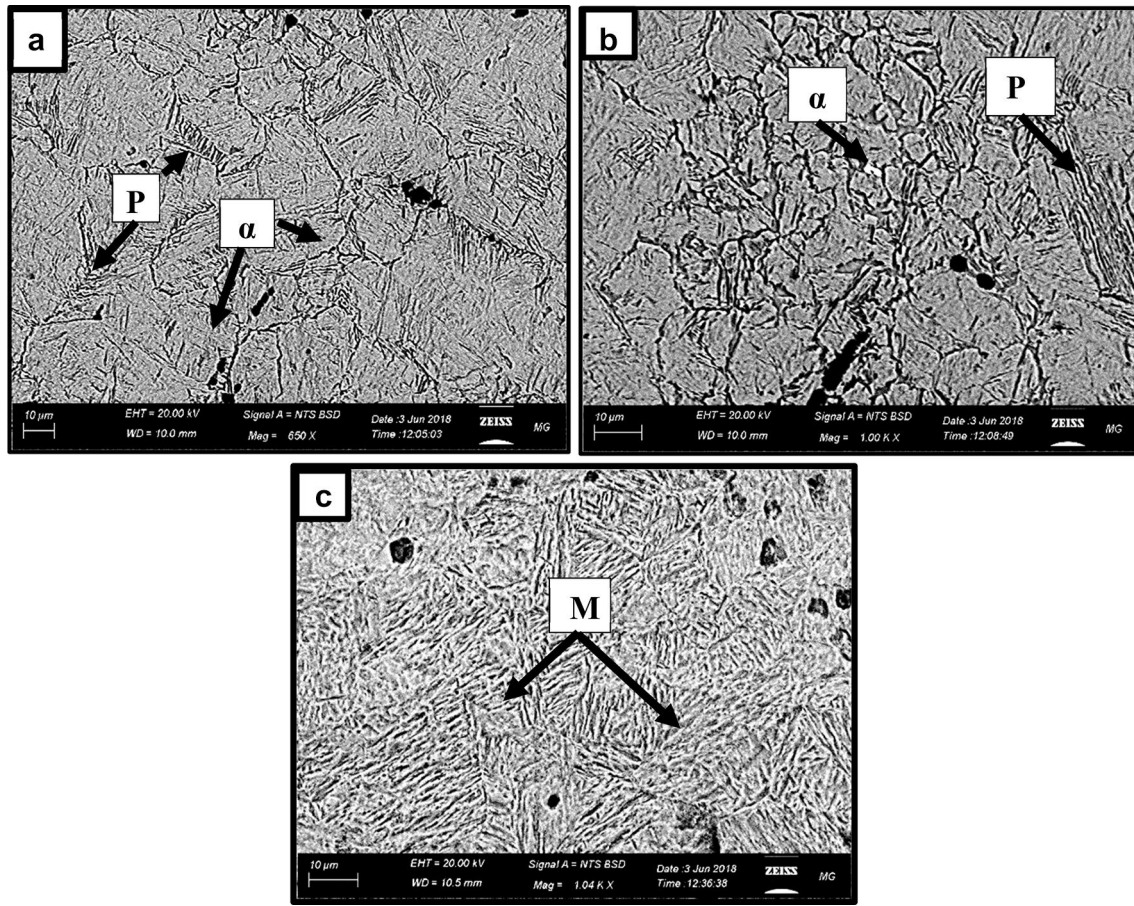


**Fig. 4** SEM micrograph of DIN50Cr3 specimens after **a** annealing R1, **b** normalizing R2 and **c** hardening R3

**Table 2** Hardness values of tempered steel using LIBS calibration and Vickers technique

Regime	Hardness estimation deduced from Fig. 3a	Hardness estimation deduced from Fig. 3b	Hardness estimation deduced from Fig. 3c	Hardness estimation deduced from Fig. 3d	Vickers mechanical hardness
R4	420 ± 0.86	420 ± 2.54	424 ± 0.86	427 ± 0.41	432
R5	408 ± 2.39	406 ± 3.30	406 ± 2.37	406 ± 1.8	410
R6	398 ± 0.47	399 ± 2.63	386 ± 1.36	386 ± 1.2	392

### 3.4 Microstructural evaluation of the tempered spring steel

The variations of the hardness values of tempered spring steel specimens can be related to the microstructural variations accompanying these treatment regimes. Figure 6 clarifies a decrease in the amount of martensite formed by increasing the tempering temperature while maintaining the tempering time. The decrease in martensite content can be attributed to the stabilization of the structure by further decomposition of martensite with increasing the tempering temperature. Moreover, formation of ferrite ( $\alpha$ ) phase and

the intergranular cementite intermetallic compound ( $\text{Fe}_3\text{C}$ ), as shown in Fig. 6a–c, increased the structure stability, decreasing the hardness while increasing the alloy ductility.

## 4 Conclusion

In the present work, laser-induced breakdown spectroscopy (LIBS) was successfully used to estimate the mechanical hardness in HV units. LIBS calibration curves were constructed through calculation of ionic–atomic ratio of different iron emission lines for three distinct spring steel

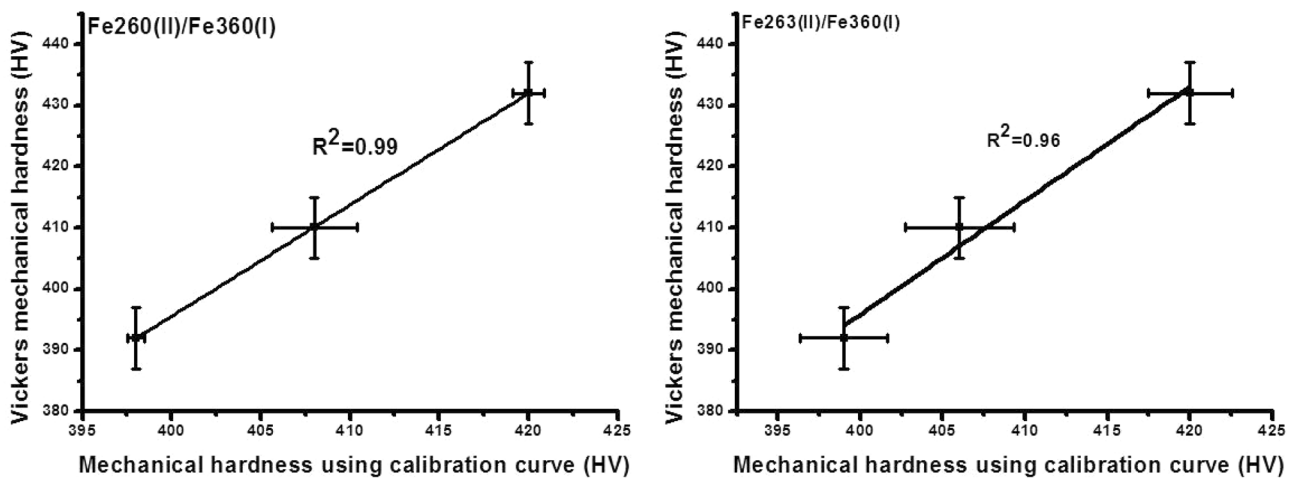


**Fig. 5** Hardness values using LIBS calibration versus the measured values using Vickers test for Fe 260 (II)/Fe 360(I) and for Fe 263 (II)/Fe 360(I)

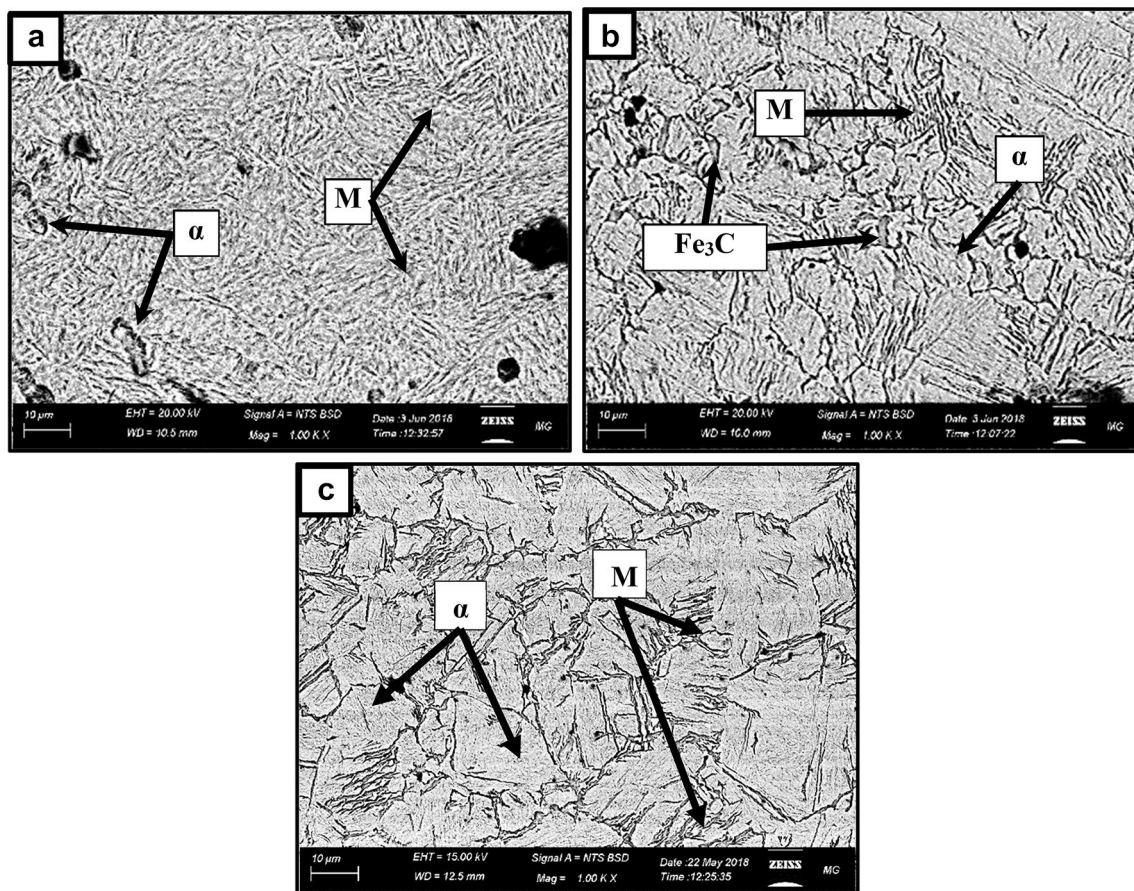


**Fig. 6** SEM micrographs of DIN 50Cr3 after tempering a R4, b R5, c R6

samples treated according to R1 annealing, R2 quenching and R3 normalizing. Besides, mechanical hardness using Vickers test and microstructural analyses were performed.

The calibration line showed that there is good proportionality ( $R^2 = 0.99$  for both shown ratios) between the ratio of ionic to atomic emission line and the mechanical hardness


measured using Vickers test. The obtained data from the calibration were used to estimate the mechanical hardness (HV units) for other three spring steel sample groups subjected to different heat treatment regimes according to R4, R5 and R6. Moreover, the hardness values obtained from the calibration were correlated with Vickers test values for the same three samples. It has been found that there is good correlation with  $R^2$  of 0.99 for Fe260(II)/Fe360(I) and 0.96 for Fe263(II)/Fe360(I). This result confirms the reproducibility of the measurement. Tempering of spring steel DIN50Cr3 reduces its hardness from 432 HV at temperature 250 °C to 392 HV at temperature 550 °C. The microstructural inspections showed that gradual decomposition of martensitic structure into the more stable ferrite and pearlite phases can be considered as the cause of reduction in the hardness values.

## References

1. D.A. Cremers, F.-Y. Yueh, J.P. Singh, H. Zhang, *Encycl. Anal. Chem. Appl. Theory Instrum.* (2006)
2. J.M. Vadillo, J.J. Laserna, *Spectrochim. Acta Part B At. Spectrosc.* **59**, 147–161 (2004)
3. A. Hussein, A. Marzouk, M. Harith, *Spectrochim. Acta Part B* **113**, 93–99 (2015)
4. S.M. Aberkane, M. Abdelhamid, K. Yahiaoui, C. Mahieddoune, S. Abdelli-Messaci, M.A. Harith, *Thin Solid Films* **653**, 293–300 (2018)
5. S.M. Aberkane, M. Abdelhamid, F. Mokdad, K. Yahiaoui, S. Abdelli-Messaci, M.A. Harith, *Anal. Methods* **9**, 3696–3703 (2017)
6. A.M. Mostafa, S.A.E.K.M. Hamed, H. Afifi, S. Mohamady, *Appl. Phys. A* **125**(8), 559 (2019)
7. M.M. ElFaham, A.M. Mostafa, G.M. Nasr, *J. Mol. Struct.* **1201**, 127211 (2020). <https://doi.org/10.1016/j.molstruc.2019.127211>
8. M. Hassan, M. Abdelhamid, O.A. Nassef, M. Abdel-Harith, *An Int. J.* **27**, 485–500 (2018)
9. M. Hassan, M. Sighicelli, A. Lai, F. Colao, A.H.H. Ahmed, R. Fantoni, M.A. Harith, *Spectrochim. Acta Part B At. Spectrosc.* **63**, 1225–1229 (2008)
10. M. Abdelhamid, S. Grassini, E. Angelini, G.M. Ingo, M.A. Harith, *Spectrochim. Acta Part B At. Spectrosc.* **65**, 695–701 (2010)
11. A. Elhassan, A. Giakoumaki, D. Anglos, G.M. Ingo, L. Robbiola, M.A. Harith, *Spectrochim. Acta Part B At. Spectrosc.* **63**, 504–511 (2008)
12. V. Lazic, S. Jovicevic, R. Fantoni, F. Colao, *Spectrochim. Acta Part B At. Spectrosc.* **62**, 1433–1442 (2007)
13. M.M. ElFaham, M. Okil, A.M. Mostafa, *Opt. Laser Technol.* **108**, 634–641 (2018). <https://doi.org/10.1016/j.optlastec.2018.07.022>
14. Z. Ramezani, S.M.R. Darbani, A.E. Majd, *Appl. Opt.* **56**(24), 6917–6922 (2017). <https://doi.org/10.1364/ao.56.006917>
15. J.S. Cowpe et al., *Spectrochim. Acta Part B At. Spectrosc.* **66**(3–4), 3–4 (2011). <https://doi.org/10.1016/j.sab.2011.03.007>
16. J.J. Gilman, *Chemistry and physics of mechanical hardness* (Wiley, New York, 2009)
17. V.N. Lednev et al., *J. Phys. Conf. Ser.* **1109**, 012050 (2018). <https://doi.org/10.1088/1742-6596/1109/1/012050>
18. M.M. ElFaham, A.M. Alnozahy, A. Ashmawy, *Mater. Chem. Phys.* **207**, 30–35 (2018). <https://doi.org/10.1016/j.matchemphys.2017.12.036>
19. K. Tsuyuki, S. Miura, N. Idris, K.H. Kurniawan, T.J. Lie, K. Kagawa, *Appl. Spectrosc.* **60**, 61–64 (2006)
20. Z.A. Abdel-Salam, A.H. Galmed, E. Tognoni, M.A. Harith, *Spectrochim. Acta Part B At. Spectrosc.* **62**, 1343–1347 (2007)
21. Z.A. Abdel-Salam, Z. Nanjing, D. Anglos, M.A. Harith, *Appl. Phys. B* **94**, 141–147 (2009)
22. M.M. ElFaham, M. Okil, N.M. Nagy, *Opt. Laser Technol.* **106**, 69–75 (2018). <https://doi.org/10.1016/j.optlastec.2018.03.018>
23. S.M. Aberkane, A. Bendib, K. Yahiaoui, S. Boudjemai, S. Abdelli-Messaci, T. Kerdja, S.E. Amara, M.A. Harith, *Appl. Surf. Sci.* **301**, 225–229 (2014)
24. D.V. Wilson, B. Russell, *Acta Metall.* **8**, 468–479 (1960)
25. D.H.L. Ng, K.S. Cho, M.L. Wong, S.L.I. Chan, X.-Y. Ma, C.C.H. Lo, *Mater. Sci. Eng. A* **358**, 186–198 (2003)
26. K.E. Thelning (ed.), *Steel and Its Heat Treated* (Butterworth-Heinemann, Oxford, 2013)
27. A.N. Isfahany, H. Saghafian, G. Borhani, *J. Alloys Compd.* **509**, 3931–3936 (2011)
28. A.K. Srivastava, G. Jha, N. Gope, S.B. Singh, *Mater. Charact.* **57**, 127–135 (2006)
29. M.S. Htun, S.T. Kyaw, K.T. Lwin, *J. Met. Mater. Miner.* **18**, 191–197 (2008)
30. W.D. Callister, Jr., D.G. Rethwisch, *Materials Science and Engineering*, 9th edn, SI version (2014). ISBN: 978-1-118-31922-2
31. Mohamed M. ElFaham, Usama Eldemerdash, *Opt. Laser Technol.* **111**, 338–346 (2019)
32. H. Kuhn, D. Medlin, *Mechanical Testing and Evaluation*, ASM Handbook, vol. 8 (2000) ISBN: 978-0-87170-389-7
33. Z.A. Abdel-Salam et al., *Spectrochimica Acta Part B* **62**, 1343–1347 (2007). <https://doi.org/10.1016/j.sab.2007.10.033>
34. S. Messaoud-Aberkane et al., *Spectrochim. Acta Part B* **113**, 147–151 (2015). <https://doi.org/10.1016/j.sab.2015.09.012>
35. A.M. Popov, T.A. Labutin, N.B. Zorov, *Mosc. Univ. Chem. Bull.* **64**(6), 366–377 (2009). <https://doi.org/10.3103/S0027131409060030>

**Publisher's Note** Springer Nature remains neutral with regard to jurisdictional claims in published maps and institutional affiliations.

## Affiliations

Mohamed M. ElFaham<sup>1</sup>  · Waled M. Elthalabawy<sup>2</sup> · O. Elzahed<sup>2</sup> · Mohamed A. Zakaria<sup>3</sup> · M. Abdelhamid<sup>4</sup>

✉ Mohamed M. ElFaham  
dr.mmostafa.elfaham@bhit.bu.edu.eg

<sup>1</sup> Department of Engineering and Basic Science, Benha Faculty of Engineering, Benha University, Benha 13518, Egypt

<sup>2</sup> Department of Material Science and Technology, Military Technical College, Cairo 11766, Egypt



<sup>3</sup> Spectroscopy Department, Laser Technology Unit, Centre of Excellence for Advanced Sciences, National Research Center, Cairo 12622, Egypt

Enhanced Sciences (NILES), Cairo University, Giza 12613, Egypt

<sup>4</sup> Department of Laser Applications in Metrology, Photochemistry and Agriculture, National Institute of Laser